Journal of Molecular Spectroscopy 281 (2012) 51–62

Contents lists available at SciVerse ScienceDirect

Journal of Molecular Spectroscopy

journal homepage: www.elsevier.com/locate/jms

High-resolution infrared studies of the ν_{10}, ν_{11}, ν_{14}, and ν_{18} levels of [1.1.1]propellane

Robynne Kirkpatrick [a], Tony Masiello [b], Matthew Martin [a], Joseph W. Nibler [a,*], Arthur Maki [c], Alfons Weber [d], Thomas A. Blake [e]

[a] Department of Chemistry, Oregon State University, Corvallis, OR 97332-4003, USA
[b] Department of Chemistry and Biochemistry, California State University, East Bay, Hayward, CA 94542, USA
[c] 15012 24th Ave., Mill Creek, WA 98012, USA
[d] Sensor Science Division, National Institute of Standards and Technology, Gaithersburg, MD 20899, USA
[e] Pacific Northwest National Laboratory, P.O. Box 999, Mail Stop K8-88, Richland, WA 99352, USA

ARTICLE INFO

Article history:
Received 27 July 2012
In revised form 3 September 2012
Available online 15 September 2012

Keywords:
Propellane
High-resolution infrared spectrum
Rovibrational constants
Coriolis interactions
Ground state structure
DFT calculations
Anharmonic frequencies

ABSTRACT

This paper is a continuation of earlier work in which the high resolution infrared spectrum of [1.1.1]propellane was measured and its k and l structure resolved for the first time. Here we present results from an analysis of more than 16000 transitions involving three fundamental bands ν_{10} $(E' - A_1')$, $\nu_{11}(E' - A_1')$, ν_{14} $(A_2'' - A_1')$ and two difference bands $(\nu_{10}-\nu_{18})$ $(E'-E'')$ and $(\nu_{11} - \nu_{18})$ $(E' - E'')$. Additional information about ν_{18} was also obtained from the difference band $(\nu_{15} + \nu_{18}) - \nu_{18}$ $(E' - E'')$ and the binary combination band $(\nu_{15} + \nu_{18})$ $(E' - A_1')$. Through the use of the ground state constants reported in an earlier paper [1], rovibrational constants have been determined for all the vibrational states involved in these bands. The rovibrational parameters for the ν_{18} (E'') state were obtained from combination–differences and showed no need to include interactions with other states. The ν_{10} (E') state analysis was also straight-forward, with only a weak Coriolis interaction with the levels of the ν_{14} (A_2'') state. The latter levels are much more affected by a strong Coriolis interaction with the levels of the nearby ν_{11} (E') state and also by a small but significant interaction with another state, presumably the ν_{16} (E'') state, that is not directly observed. Gaussian calculations (B3LYP/cc-pVTZ) computed at the anharmonic level aided the analyses by providing initial values for many of the parameters. These theoretical results generally compare favorably with the final parameter values deduced from the spectral analyses. Finally, evidence was obtained for several level crossings between the rotational levels of the ν_{11} and ν_{14} states and, using a weak coupling term corresponding to a $\Delta k = \pm 5$, $\Delta l = \mp 1$ matrix element, it was possible to find transitions from the ground state that, combined with transitions to the same upper state, give a value of $C_0 = 0.1936515(4)\ \mathrm{cm}^{-1}$. This result, combined with the value of $B_0 = 0.28755833(14)\ \mathrm{cm}^{-1}$ reported earlier [1], yields a value of 1.586277(3) Å for the length of the novel axial CC bond in propellane.

1. Introduction

[1.1.1]Propellane or, more simply, propellane (C_5H_6) is the prototype of a whole class of tricyclic organic molecules having three medial rings fused to form an axial-axial carbon single bond. The name propellane was introduced into the chemical literature by Ginsburg [2]. This unusual structure (Fig. 1) challenges us to rethink our models of how individual atoms combine to form molecules. Of greatest interest is the novel central bond that joins the axial carbon atoms; as seen in the figure, the angle between the axial bond and the carbons on each corner of the trigonal bipyramid is acute rather than obtuse. Clearly the bonding hybridization at the axial carbons differs significantly from the more normal sp, sp^2 or sp^3 types observed for carbon and hence this molecule and its derivatives have been the subject of a number of investigations [2–8]. From the outset, it was assumed that the symmetry of propellane was D_{3h} and this was confirmed by analysis of gas phase electron diffraction measurements [9] and by vibrational IR and Raman studies [10]. Our quantum calculations [1] and the detailed higher resolution spectral measurements reported here also indicate that this is the symmetry of the equilibrium structure of this simplest case of the propellanes.

Once thought to be too unstable to exist, propellane was first synthesized in 1982 by Wiberg and Walker [11]. Wiberg and coworkers [10] did an extensive study of the spectrum of propellane in the gas phase using infrared and Raman spectroscopy with spectral resolutions of 0.06 cm^{-1} and 2 cm^{-1}, respectively. They

* Corresponding author. Fax: +1 541 737 2062.
E-mail addresses: joseph.nibler@orst.edu, Niblerj@chem.orst.edu (J.W. Nibler).

0022-2852/$ - see front matter © 2012 Elsevier Inc. All rights reserved.
http://dx.doi.org/10.1016/j.jms.2012.09.001

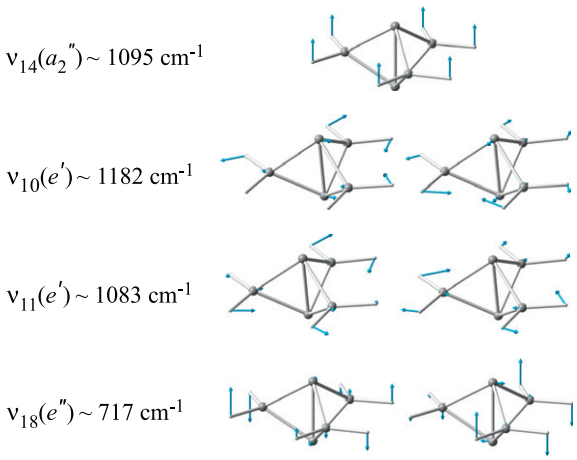

Fig. 1. Views of the ν_{10}, ν_{11}, ν_{14}, and ν_{18} normal modes of the D_{3h} structure of [1.1.1]propellane.

were able to obtain approximate values for many of the fundamental vibrational frequencies and some information about its normal coordinates and dipole derivatives. While they observed some *J* structure in several bands, they were unable to identify any *K* structure due to the relatively low instrumental resolution available at that time. The high symmetry and small size of this molecule have led us to use improved high-resolution spectroscopic and *ab initio* theoretical methods to reexamine in detail the spectral and structural properties of this intriguing molecule [1,12–14]. Such spectroscopic studies can provide accurate values of rovibronic parameters that can serve as a direct test of quantum calculations, which are often affected by the choice of basis set and computational model. Conversely, as in this work, the quantum prediction of basic rovibrational parameters can also serve as an indispensible guide in the initial analysis of complicated or congested spectra.

The work presented here deals with the determination of parameters that describe the ν_{10}, ν_{11}, and ν_{14} fundamental vibrations of propellane, obtained from an analysis of the three fundamentals as well as of the $\nu_{10} - \nu_{18}$, $\nu_{11} - \nu_{18}$ and $(\nu_{15} + \nu_{18}) - \nu_{18}$ difference bands. In this global fit, ground state parameters were fixed at values determined previously [1]. In that work the effect of any perturbations on upper states was removed by taking energy differences between pairs of transitions having the same upper levels and different lower state levels so that accurate spacings between ground state rotational levels were used in the fit. (This combination-difference method is described in Ref. [15].) Here, a similar procedure was used to obtain rovibrational parameters for the ν_{18} state. These and the ground state parameters were then held constant in a global fit of more than 16000 transitions involving the infrared-active ν_{10} (E'), ν_{11} (E'), and ν_{14} (A_2'') states. The analysis required consideration of Coriolis interactions between the ν_{10} and ν_{14} as well as the ν_{11} and ν_{14} states, and also an unusual $\Delta k = \pm 4$, $\Delta l = \pm 1$ interaction between the rotational levels of ν_{14} and a nearby infrared-inactive ν_{16} (E'') state. Furthermore, several local $\Delta k = \pm 5$, $\Delta l = \mp 1$ perturbations were identified in the spectra of ν_{14} and ν_{11} that allowed the ground state rotational parameter C_0 to be determined.

2. Experimental details

2.1. Synthesis

Using the protocol reported by Belzner and coworkers [16], propellane was produced in an ether solution under argon. Since propellane is difficult to separate from ether using fractional distillation [10], it was converted, using the protocol of Alber and Szeimies [17], to solid 1,3-diiodobicyclopentane, a relatively stable molecule that can be stored and reconverted to propellane. Reconversion to propellane was achieved by addition of sodium cyanide (in DMSO, dry) under nitrogen, with stirring for thirty minutes [17]. Pure propellane was then extracted using fractional distillation at room temperature at a pressure of 13.3 Pa (0.1 Torr). A trap cooled to −78 °C and coated with hydroquinone was used to collect the product; the hydroquinone served as a radical scavenger to reduce potential dimerization on the trap surfaces. The internal gold-coated surfaces of the 20 cm IR absorption cells employed to record some spectra were also coated with hydroquinone but this was not done with the long path White cell used and the rate of decomposition was not noticeably higher in the latter case. Hence the need for the hydroquinone coating is not clear.

2.2. Spectral measurements

Spectra were taken using Bruker 120 or 125 FTIR spectrometers at the Pacific Northwest National Laboratories.[1] The spectrometers employ a Globar light source, various detectors, and either a 20 cm absorption cell or a 1 m multipass White cell. The spectrometer optical path (except that in the absorption cell) was evacuated. Boxcar apodization was used and interferograms were collected single-sided with both forward and backward scans. Table 1 summarizes the instrumental conditions that were used for recording the spectra. Fig. 2 gives a survey view of the infrared spectrum of the region 1060–1200 cm^{-1} that contains the IR active fundamental bands ν_{10}, ν_{11}, and ν_{14}. Fig. 3 shows the relatively weak difference band $\nu_{10} - \nu_{18}$ (band origin ~ 466 cm^{-1}) while Fig. 4 similarly displays the $\nu_{11} - \nu_{18}$ band (band origin ~366 cm^{-1}); these were used to help establish both the ν_{18} and ν_{11} parameters.

3. Band analyses

3.1. Energy levels

Propellane is an oblate symmetric top for which the term energy of a given vibrational state v is given by

$$E_v = G(v,l) + F_v(J,K,l), \tag{1}$$

where $G(v,l)$ is the vibrational term, and the rotational term for non-degenerate vibrational states (i.e. $l = 0$) $F_v(J,K)$ is given by

$$\begin{aligned} F_v(J,K) = {} & B_v J(J+1) + (C_v - B_v)K^2 - D_v^J J^2(J+1)^2 - D_v^{JK} J(J \\ & + 1)K^2 - D_v^K K^4 + H_v^J J^3(J+1)^3 + H_v^{JK} J^2(J+1)^2 K^2 \\ & + H_v^{KJ} J(J+1)K^4 + H_v^K K^6 \pm \delta_{3K}\Delta_3 J(J+1)[J(J+1) - 2] \\ & \times [J(J+1) - 6] + \cdots. \end{aligned} \tag{2}$$

For doubly degenerate vibrational states the rotational term expression is given by

$$F_v(J,K,l) = F_v(J,K) + F_{v\perp}(J,k,l) \tag{3}$$

in which

$$F_{v\perp}(J,k,l) = -2(C\zeta)_v kl + \eta_v^J J(J+1)kl + \eta_v^K k_3 l + \cdots. \tag{4}$$

and, when $l = \pm 1$, the Δ_3 splitting expression of Eq. (2) is replaced by $\pm\delta_{-2(kl)}\ \Delta_2 J(J+1)[J(J+1) - 2]$. Δ_3 and Δ_2 are splitting parame-

[1] Certain commercial equipment, instruments, and materials are identified in the paper to adequately specify the experimental procedure. Such identification does not imply recommendations or endorsements by the National Institute of Standards and Technology or the Pacific Northwest National Laboratory, nor does it imply that the materials or equipment identified are necessarily the best available for the purpose.

Table 1
Experimental conditions for bands analyzed in this work. Most scans were recorded at 22.5 °C[a].

Spectral region (cm^{-1})	Pressure Pa/(Torr)	Resolution (cm^{-1})	Path length (m)	Calibration gas	Scans	Detector	Spectrometer Bruker	Band(s)
50–500	333/(2.50)	0.002	25.6	H_2O (HITRAN)	256	Bolometer	120	$\nu_{11} - \nu_{18}$
350–700	200/(1.50)	0.0015	25.6	H_2O (HITRAN)	352	Bolometer	125	$\nu_{10} - \nu_{18}$, $(\nu_{15} + \nu_{18}) - \nu_{18}$
500–1800	68/(0.51)	0.0018	12.8	N_2O (NIST)	128	MCT (Mid)	125	ν_{14}, ν_{11}
1090–3620	63/(0.47)	0.0025	25.6	OCS (NIST)	640	MCT (Mid)	125	ν_{10} ($\nu_{15} + \nu_{18}$)

[a]Some scans of the intense ν_{14} band were taken in a 20 cm cell cooled to −10.0 °C.

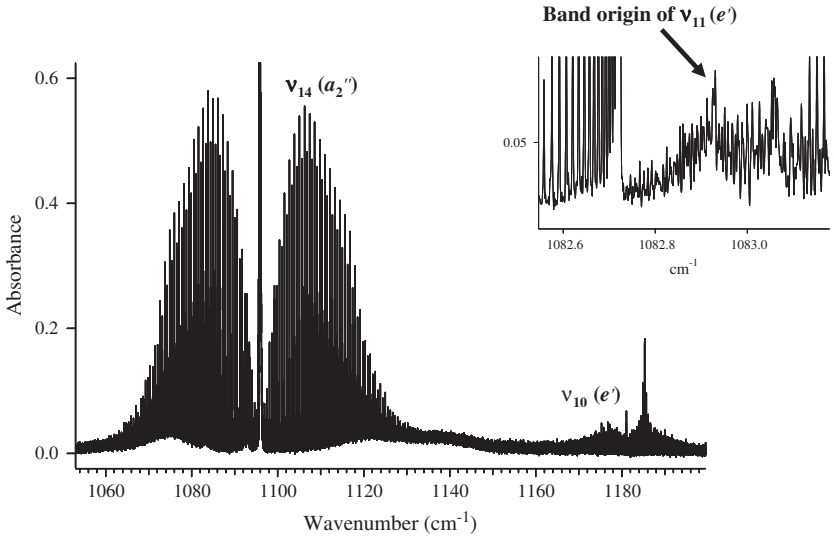

Fig. 2. Overview of the propellane spectrum from 1050 to 1200 cm^{-1}. This spectrum was recorded at a pressure of 133 Pa (1 Torr) and temperature of −10 °C using a 20 cm absorption cell. The strong band at 1096 cm^{-1} is ν_{14}. The band origin of ν_{11} is located at 1083 cm^{-1}. The ν_{10} band is located at 1182 cm^{-1}.

ters; for molecules with a threefold symmetry axis, Δ_3 in the ground state should be close to the h_3 constant given by the Gaussian program and Δ_2 is zero. For degenerate vibrational levels, Δ_2 is an effective constant that characterizes splitting of the $kl = -2$ levels.

In these expressions J is the total angular momentum quantum number, k is the signed quantum number for the projection of the vector **J** onto the symmetry axis, $K = |k|$, and l is the vibrational angular momentum quantum number. The quantities C and B are proportional to the expectation values of the inverse moments of inertia for rotation about z (the top axis) and an x or y axis in the equatorial plane of the molecule, respectively. The $(C\zeta)_v$ term in Eq. (4) accounts for the intra-vibrational Coriolis interactions; when the product kl is positive (negative) the vibrational and rota-

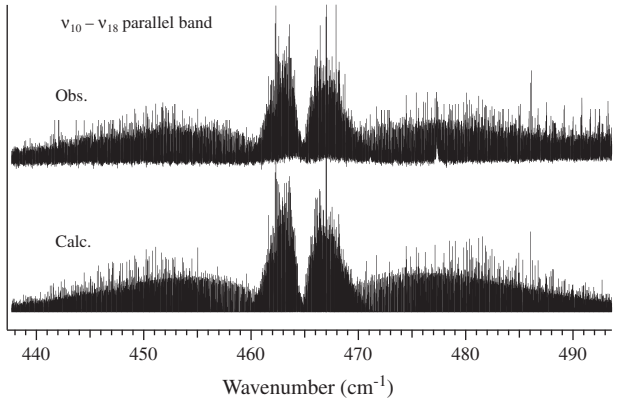

Fig. 3. The $\nu_{10} - \nu_{18}$ band of propellane. (Some strong isolated lines due to water vapor absorption have been masked.)

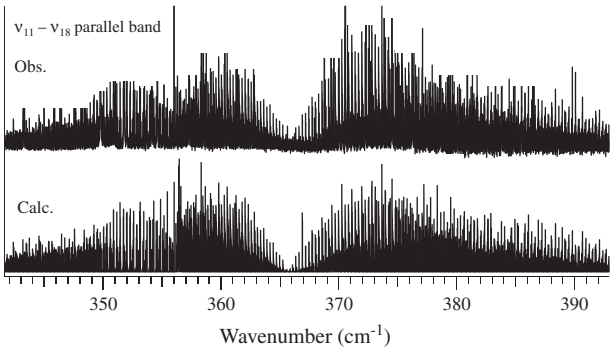

Fig. 4. The $\nu_{11} - \nu_{18}$ band of propellane. (Some strong isolated lines due to water vapor absorption have been masked.)

tional angular momenta are parallel (antiparallel). The contracted subscript v is used to represent both quantum number and mode number of a vibrational state. For the ground state $\nu_1 = \nu_2 = \nu_3 = \cdots = 0$. The zero energy is defined as the $J = K = 0$ level of the ground state so that $\nu_0 = G(v,l) - G(0,0)$.

In addition to the above, an off-diagonal l-type resonance term is included that has the primary effect of splitting the $kl = 1$ levels of a degenerate vibrational state with $l = \pm 1$. This term is defined as

$$\begin{aligned} W_{22} &= \langle \nu, J, k, l | H | v, J, k \pm 2, l \pm 2 \rangle \\ &= 1/4\{q + q_J J(J+1) + q_k[k^2 + (k \pm 2)^2]\} \times [(v+1)^2 - (l \pm 1)^2]^{1/2}[J(J+1) - k(k \pm 1)]^{1/2}[J(J+1) - (k \pm 1)(k \pm 2)]^{1/2} \end{aligned} \quad (5)$$

where H is the Hamiltonian operator of the interaction. This term also pushes apart other pairs of levels for which $\Delta k = \Delta l = \pm 2$ but, since these levels are already separated by other terms, the effect is minimal compared with that on the otherwise degenerate $kl = 1$ levels. Sometimes the fits are improved by including the q_J and q_k terms which represent the effect of the centrifugal distortion, as do the D, H, and η parameters in Eqs. (2) and (4).

Another important interaction that can have a profound effect on the spectra is the Coriolis coupling between states whose product symmetry is that of a rotation (Jahn's rule). Such an interaction is expected for each A_2'' and E' pair of vibrational states considered here since the E'' product symmetry corresponds to the symmetry of the R_x, R_y rotations. Several such interactions can occur between the various states displayed in Fig. 5, which shows our best estimate of the actual positions of the vibrational levels in the 1000–1200 cm^{-1} region. As discussed in Refs. [18,19], the Coriolis interaction results in an off-diagonal term which, in the case of the ν_{14} (A_2'') and ν_{11} (E') states of propellane, can be written

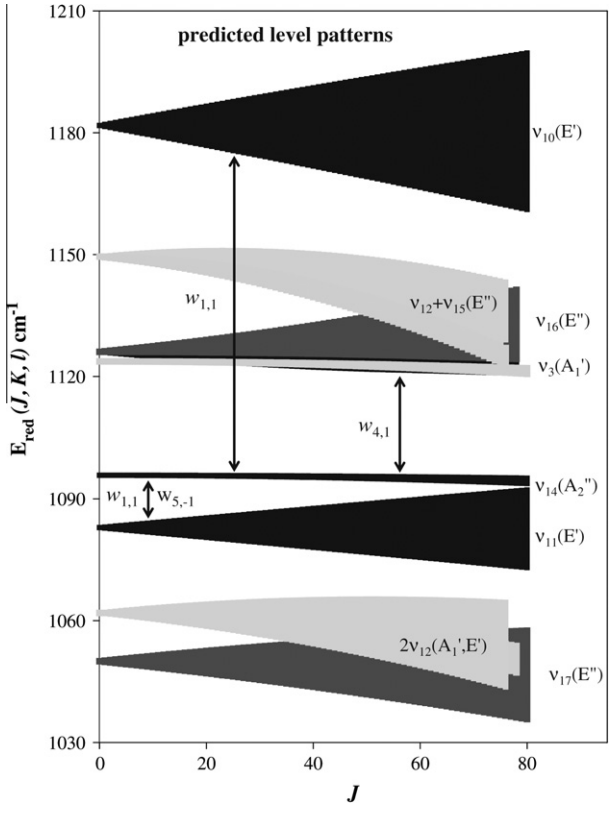

Fig. 5. Reduced energy level diagram in the ν_{10}, ν_{11}, and ν_{14} region. Not shown are the ν_{18} levels which are relatively isolated at about 720 cm^{-1}.

$$\begin{aligned} W_{1,1} &= \langle \nu_{11}, \nu_{14}, J, k, l_{11} | H | \nu_{11} + 1, \nu_{14} - 1, J, k \pm 1, l_{11} \pm 1 \rangle \\ &= \pm 2^{1/2} \Omega_{14,11} B \zeta^{y}_{14,11t2}[J(J+1) - k(k \pm 1)]^{1/2} \\ &\quad + \text{higher terms} \\ &= \pm\{w_{1,1} + w_{1,1,J} J(J+1) + w_{1,1,k}[k^2 + (k \pm 1)^2] + w_{1,1,kl}[kl \\ &\quad + (k \pm 1)(l \pm 1)]\}[J(J+1) - k(k \pm 1)]^{1/2} \end{aligned} \quad (6)$$

where $\Omega_{14,11} = \frac{1}{2}[(\omega_{11}/\omega_{14})^{1/2} + (\omega_{14}/\omega_{11})^{1/2}] \approx \frac{1}{2}[(\nu_{11}/\nu_{14})^{1/2} + (\nu_{14}/\nu_{11})^{1/2}]$ is very close to 1 and is subsumed in the fitted parameter $w_{1,1}$. A similar relation applies for the ν_{14} and ν_{10} interaction. In calculating $w_{1,1}$ from theoretical results, we have used harmonic ω values, $B \approx B_e$ and $\zeta^{y}_{14,11t2}$, where the t_2 subscript refers to the degenerate component of ν_{11} that is antisymmetric with respect to reflection through a y–z plane. We note that, when the y axis contains one of the equatorial C atoms, the degenerate coordinates naturally have the appropriate symmetry and $\zeta^{y}_{14,11t21} = \zeta^{x}_{14,11t2} = 0$. The possible higher order terms $w_{1,1,J}$ and $w_{1,1,k}$ are centrifugal distortion corrections and $w_{1,1,kl}$ is also a higher-order Coriolis interaction correction.

Finally, two other less common off-diagonal terms proved necessary to account for some of the perturbations seen in the ν_{11} and ν_{14} spectra. The first of these is a small $\Delta k = \pm 4$, $\Delta l = \pm 1$ $W_{4,1}$ interaction term that couples the ν_{14} levels with those of the slightly higher ν_{16} state. This term results in mixing of the ν_{14} and the ν_{16} rovibrational states via the matrix element

$$\begin{aligned} W_{4,1} &= \langle v_{16}, v_{14}, J, k, l_{16} | H | v_{16} - 1, v_{14} + 1, J, k \pm 4, l_{16} \pm 1 \rangle \\ &= \{w_{4,1} + w_{4,1,J} J(J+1) + w_{4,1,k}[k^2 + (k \pm 1)^2]\} \times \{[J(J+1) \\ &\quad - k(k \pm 1)][J(J+1) - (k \pm 1)(k \pm 2)] \times [J(J+1) - (k \pm 2) \\ &\quad \times (k \pm 3)][J(J+1) - (k \pm 3)(k \pm 4)]\}^{1/2}. \end{aligned} \quad (7)$$

We note that, since ν_{16} is infrared inactive and is very likely mixed with the nearby ν_3 (A_1') and ($\nu_{12} + \nu_{15}$) (E'') states, the ν_{16} constants deduced from our analysis must be regarded mainly as fitting parameters.

The second off-diagonal term is a more localized $\Delta k = \pm 5$, $\Delta l = \mp 1$ $W_{5,-1}$ interaction term that mixes the ν_{11} and ν_{14} rovibrational states. Though small in magnitude, it is important due to the close proximity of some of the ν_{11} and ν_{14} rotational levels and, as discussed later, the perturbations that it produces allow us to determine the C_0 ground state constant. Except in special cases [20], that parameter is normally unavailable from the fundamental bands of infrared spectra of symmetric tops that do not show evidence of such an interaction. The matrix element for this $W_{5,-1}$ term is

$$\begin{aligned} W_{5,-1} &= \langle \nu_{11}, \nu_{14}, J, k, l_{11} | H | \nu_{11} - 1, \nu_{14} + 1, J, k \pm 5, l_{11} \mp 1 \rangle \\ &= \{w_{5,-1} + w_{5,-1,J} J(J+1) + w_{5,-1,k}[k^2 + (k \pm 1)^2]\} \\ &\quad \times \{[J(J+1) - k(k \pm 1)][J(J+1) - (k \pm 1)(k \pm 2)][J(J+1) \\ &\quad - (k \pm 2)(k \pm 3)][J(J+1) - (k \pm 3)(k \pm 4)][J(J+1) \\ &\quad - (k \pm 4)(k \pm 5)]\}^{1/2}. \end{aligned} \quad (8)$$

Fig. 5 shows all of the interactions included in our fitting model but a number of other couplings were also considered. For example, Fermi resonance between ν_{11} (E') and $2\nu_{12}$ (E') will occur but is assumed to be incorporated into the effective band origin (ν_0) value for ν_{11}. Coriolis mixing will occur between ν_{11} (E') and the ν_{16} (E''), ν_{17} (E'') states, as well as between the ν_3 (A_1') and ν_{17} (E'') levels. The result of these and other interactions will be to produce a blend of many of the states shown in Fig. 5. Many coupling models were explored [14] but, remarkably, the relatively simple model using the interactions shown in boldface in the figure proved sufficient to fit very accurately more than 16000 transitions to the ν_{10}, ν_{11}, and ν_{14} states.

3.2. Intensity calculations

As part of the analysis, spectral simulations were a valuable aid in making assignments [14]. For a transition of wavenumber value ν that originates from a ground state level J'', K'', $l = 0$ of wavenumber energy E'' and terminates on an upper state with quantum number J', K', l', the intensity is given by

$$I(J'',K'',0;J',K',l') = Cg_{\mathrm{ns}}(2J+1)\nu(1-e^{-hc\nu/(k_BT)})e^{-hcE''/(k_BT)}|\mu_{\psi'\psi''}|^2, \quad (9)$$

where C is a scaling parameter that can be 1 for relative comparisons within a given spectrum, g_{ns} is the nuclear spin statistical weight of the initial state, and $\mu_{\psi'\psi''}$ is the transition moment whose square is proportional to the usual Hönl–London factors [21]. For the ground state of propellane g_{ns} is 24 for K = multiples of 3 and 20 otherwise except for $K = 0$, where the weight is 16 for odd J (levels with A_2' or A_2'' rovibrational symmetry) and 8 for even J (levels with A_1' or A_1'' rovibrational symmetry) [22]. Intensity variations caused by g_{ns} proved quite helpful in making assignments and in deducing the signs of some of the splitting parameters. Similarly, in the event of mixing, the upper state is a linear combination of the interacting states and interference effects can occur due to the $|\mu_{\psi'\psi''}|^2$ factor. Transitions to such mixed states can be identified by their intensity deviation from values given by Eq. (9) and analysis of these can sometimes lead to useful information about the relative signs and magnitudes of dipole derivatives for the coupled modes of vibration [12,14,18].

4. Results and discussion

4.1. Quantum calculations

All theoretical calculations of the properties of propellane were done using the Gaussian 09 electronic structure program, version B.01, at the B3LYP density functional level using the cc-pVTZ basis set [23]. These calculations give structural parameters corresponding to the equilibrium D_{3h} configuration and quadratic force constants in the potential about this energy minimum, from which one obtains the harmonic vibrational frequencies (ω's), normal modes (Q's), quartic centrifugal distortion constants (D's), and Coriolis constants (ζ_{ij}'s), as well as infrared and Raman intensities for the fundamental bands. By invoking the Anharm option, the program computes cubic and quartic force constants that give anharmonicity corrections (x_{ij}'s) that yield anharmonic frequencies (ν's) that are generally much closer to the values observed for the fundamental modes. For symmetric tops, some anharmonicity corrections have resonance terms that give unreasonable and even negative prediction of the ν's. However this problem can be avoided by a procedure proposed by Willetts and Handy [24], in which the symmetry of the molecule is lowered somewhat by a slight extension of one or more bonds. In the case of propellane, this was done by increasing two C–H bond lengths by 0.0001 Å, such that the molecule was an asymmetric top with symmetry C_{2v}. This produces slightly different frequencies for degenerate modes that were then averaged. We note that the Gaussian program also corrects for any remaining cases of Fermi or other resonances, by dropping the offending terms in the anharmonicity expressions, yielding so-called "deperturbed" ν^* values. The resonant terms are then used as off-diagonal elements in 2×2 matrix calculations that give anharmonic frequencies ν that can be compared to the observed frequencies. Table 2 compares the results of these calculations, along with the infrared and Raman intensities, with the experimental values available from this work and the references cited in the table.

Additionally, with the VibRot option in Gaussian, the quadratic and cubic constants yield sextic distortion constants (H's) and vibration-rotation interaction constants (α's). These calculations can be done for the undistorted D_{3h} molecule. In the case of the α's, resonances can occur when two modes that can Coriolis couple are of similar frequency. Gaussian accounts for this resonance if the frequency difference is less than 10 cm^{-1} but does not explicitly indicate this in the output. (For more discussion of this, and of the calculation of the l-doubling constants q of Eq. (5), see Appendix A of Ref. [25].) In computing the D's and H's, some care is required in ensuring that the z-axis is aligned along the symmetry axis of the top. This can be achieved by specifying the structure in appropriate Cartesian coordinates and using the Nosym option

Table 2
Frequencies (cm^{-1}) and relative intensities of the fundamental modes of propellane.

Mode		Experiment[a]	Theory[b]			
Symmetry	Number		Harmonic	Anharmonic	Relative intensity[c]	
					Raman	IR
a_1'	1	3029.1	3130.9	3022.9 ***2998.2***	324 vs	–
	2	1502.7	1541.1	1516.7	2.8 w	–
	3	1123.7	1152.7	1117.7 ***1099.0***	64 vs	–
	4	**907.74**	917.9	901.8	12.6 s	–
a_2'	5	–	3207.7	3063.8	–	–
a_2'	6	–	968.9	954.6	–	–
e'	7	3079.9	3210.5	3066.1	95 m	10.9 s
	8	3019.6	3125.5	2993.3 ***3028.3***	0.3	24 s
	9	**1459.21**	1494.5	1458.0 ***1453.1***	3.3	2.7 m
	10	**1181.80**	1221.1	1187.5 ***1163.1***	4.5 vw	1.1 w
	11	**1082.90**	1101.2	1071.4	6.4 vw	1.2 vw
	12	**531.50**	532.6	528.8	0.8 w	0.2 w
a_1''	13	–	918.6	891.8	–	–
a_2''	14	**1095.79**	1120.0	1091.8	–	76
a_2''	15	**612.32**	601.4	565.6	–	128 vs
e''	16	**1122.70**	1151.7	1119.5	8.8 vw	–
	17	1064.3	1078.4	1051.1	0.8 vw	–
	18	**717.12**	712.2	682.6	0.7 w	–

[a] Experimental frequencies in bold face are from Refs. [12,13] and this work. The other frequencies are from Ref. [10].
[b] This work, B3LYP/cc-pVTZ calculations using Gaussian 09 with Anharm/Vibrot options. Anharmonic frequencies in bold italics are from Gaussian and include shifts caused by Fermi resonance.
[c] The qualitative experimental intensities (vw, w, m, s, vs), where available, are taken from Ref. [10].

Table 3
Ground state parameters (cm^{-1}) of propellane.

Parameter	Expt.[a]	Theory[b]
B_0	0.28755833(14)	0.28655
C_0	0.1936515(4)	0.19178
$D_J \times 10^7$	1.1313(5)	1.147
$D_{JK} \times 10^7$	−1.2633(13)	−1.285
$D_K \times 10^7$	0.4199(13)	0.424
$H_J \times 10^{12}$	0.072(4)	0.072
$H_{JK} \times 10^{12}$	−0.224(13)	−0.441
$H_{KJ} \times 10^{12}$	0.225(15)	0.621
$H_K \times 10^{12}$	[−0.247]	−0.247
$\Delta_3 \times 10^{12}$		0.0118

[a] Ground state values are taken from Ref. [1]. The C_0 value is from the current study. Uncertainties (two standard deviations) are given in parentheses. The entries in brackets were fixed to the theoretical values.

[b] Theoretical values are computed with the Gaussian 09W program (B3LYP/cc-pVTZ). ($\Delta_3 = h_3$) The D and H parameters are for the equilibrium structure. The theoretical H parameters in Ref. [1] are incorrect and should be replaced by the values given here.

[26]. Table 3 gives the resultant theoretical ground state constants of propellane, which are identical to those we reported in Ref. [1], with two exceptions. First, the theoretical H values given here do correspond to the correct axis choice, whereas the H values of Ref. [11] do not. This error is of no great consequence since it does not change any of the experimental values which in fact are in better accord with the corrected H results. The second change in Table 3 is the listing of experimental C_0 and D_K parameters determined in the present work. This too does not change any of the analyses done in Refs. [1,12–14].

The rovibrational parameters obtained from these quantum calculations proved quite useful in the initial stages of the band analyses done in this work. For example, the pattern of rovibrational levels in the ν_{10}, ν_{11}, ν_{14} region of interest are shown in Fig. 5. Here $E_{red} = E'(J,K,l) - E''(J,K,0)$ is plotted versus J, with the range of K values up to J, and with the shape of the "wedges" determined by the theoretical values of $C'\zeta$, $\Delta B = B' - B''$ and $\Delta C = C' - C''$. The origins are our best estimates from theory or from the experimental values of the v's where available. This display also indicates those interactions between levels that our analysis finds are most significant. The $w_{1,1}$ parameters defined in Eq. (6) account for Coriolis interactions of ν_{14} levels with those of ν_{10} and ν_{11} and these can be estimated from the theoretical results. From these values and the level separations of the figure, we expect that the ν_{11} and ν_{14} levels will be strongly perturbed but those of ν_{10} will be relatively unaffected. Similarly, the ν_{18} (e'') levels near 712 cm^{-1} (not shown in the figure) should be even less perturbed since they are well-removed from the nearest levels, ν_{15} (a_2'') at 612 cm^{-1} and ν_{13} (a_1'') at about 884 cm^{-1}, neither of which can Coriolis couple with ν_{18}.

Although useful in making preliminary judgments about the levels that are most likely to interact, the reduced energy displays of Fig. 5 are deceptive in that they do not correctly show the separations of interacting levels of different K value. For example, for a given Δk, Δl interaction, a better indication of the separation of the relevant levels of modes 14 and 11 is $E_{int} = E_{11}(J,K+\Delta k,l+\Delta l) - E_{14}(J,K,l)$. For the region of interest, we find that the most important interactions are the $w_{1,1}$ Coriolis coupling of ν_{14} with the $kl < 0$ levels of ν_{11} and the $w_{4,1}$ coupling of ν_{14} with the $kl < 0$ levels of ν_{16}. Level crossings of ν_{14} and ν_{16} are predicted to occur for J values above about 40 and, indeed, perturbations due to such level crossings are observed in the ν_{11} and ν_{14} spectra, as discussed in a later section.

4.2. ν_{10} (e') analysis

Fig. 1 shows the components of the degenerate ν_{10} normal mode from the GaussView representation and these suggest that this mode is mainly an antisymmetric rocking motion of the CH_2 units. However the normal mode representations from Gaussian tend to overemphasize the large amplitude H-atom motions and the more detailed normal coordinate calculations of Wiberg et al. [10] suggest that the mode is better described as an e'-type antisymmetric stretching of the non-axial CC bonds (53%) mixed with 17% CH_2 rock.

Since the ν_{10} levels are relatively isolated, the fit of the transitions of the ν_{10} perpendicular band was straightforward, with the $^rQ_0$ band easily identified because of the characteristic intensity alternation of the odd and even J lines, as shown in Fig. 6. 5100

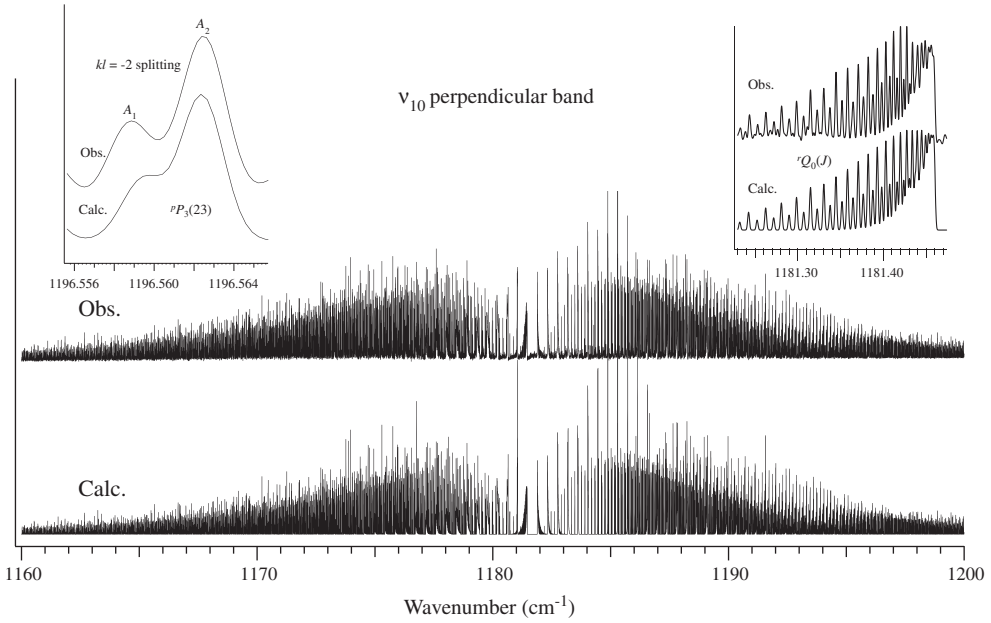

Fig. 6. The ν_{10} band of propellane. The inset on the right shows the intensity variation due to nuclear spin weights for $^rQ_0$. The inset on the left shows the splitting in the $^pP_3(23)$ transition due to splitting of the $K' = 2$ levels of the upper state.

fundamental lines were assigned and fitted and an additional 3471 lines from the $\nu_{10} - \nu_{18}$ difference band were subsequently included in arriving at the ν_{10} rovibrational parameters in the second column of Table 4. The Gaussian calculations predict a value of $w_{1,1} = 0.092\ cm^{-1}$ for the Coriolis coupling between ν_{10} and ν_{14}. When this coupling was included in the analysis, only very small changes occurred, mainly in the ΔB_{10}, q_{10} and ΔB_{14} values, and the standard deviation of the fit was not significantly improved. Hence the ν_{10} parameters listed in the table correspond to the uncoupled case, $w_{1,1} = 0$. In general, the experimental ν_0, ΔC, and $(C\zeta)$ values agree well with the theoretical predictions for ν_{10}. The somewhat poorer agreement seen for ΔB and q is due in part to the neglect of the Coriolis coupling of ν_{10} and ν_{14}.

4.3. ν_{18} (e'') analysis

The GaussView representation of ν_{18} is shown in Fig. 1 and according to Ref. [10] this mode, like ν_{10}, is best characterized as an antisymmetric stretching of the non-axial CC bonds (78%) mixed with 20% CH_2 rock, with the internal coordinate combinations both of e'' symmetry. The fundamental band is infrared inactive but is Raman active and has been assigned as an unresolved weak feature at $713.9\ cm^{-1}$ in the Raman spectrum of the gas phase [10]. This value is in reasonable agreement with our more accurate value of $717.12\ cm^{-1}$ deduced from three infrared difference bands $\nu_{10} - \nu_{18}$, $\nu_{11} - \nu_{18}$ and $(\nu_{15} + \nu_{18}) - \nu_{18}$, as described below. As mentioned earlier, the Gaussian calculations suggest that the ν_{18} levels should be relatively unperturbed and the band analyses are in accord with this.

Table 4
Rovibrational parameters (cm^{-1}) of the ν_{10} and ν_{18} vibrational states of propellane.

Parameter[a]	ν_{10} (e')		ν_{18} (e'')	
	Experiment[b,c]	Theory	Experiment[b,c]	Theory
ω_0		1221.1		712.2
ν_0	1181.79513(2)	1163.1	717.12438(2)	682.6
$\Delta C \times 10^3$	−0.22324(6)	−0.206	−0.37763(5)	−0.371
$\Delta B \times 10^3$	0.04241(5)	0.065	−0.89811(6)	−0.873
$\Delta D_J \times 10^8$	0.696(4)		−0.543(3)	
$\Delta D_{JK} \times 10^8$	−2.387(10)		1.381(8)	
$\Delta D_K \times 10^8$	1.515(7)		−0.836(6)	
$\Delta H_J \times 10^{12}$	0.214(8)			
$\Delta H_{JK} \times 10^{12}$	−1.07(3)			
$\Delta H_{KJ} \times 10^{12}$	0.80(2)			
$\Delta H_K \times 10^{12}$				
$\Delta_2 \times 10^8$	−0.4325(12)		−0.387(7)	
(Cz)	0.1202468(7)	0.1353	0.0778635(6)	0.0792
$\eta_J \times 10^5$	0.4465(2)		0.1012(3)	
$\eta_K \times 10^5$	−0.3770(2)		−0.1022(3)	
$\eta_{JK} \times 10^9$	0.135(3)			
$\eta_{KK} \times 10^9$	−0.129(2)			
$\eta_{JJK} \times 10^{14}$	0.51(3)			
$\eta_{KKK} \times 10^{14}$	−0.44(3)			
$q \times 10^3$	−0.2648(2)	−0.327	−0.9113(2)	−0.917
$q_J \times 10^8$	0.297(7)		0.34(2)	
$q_K \times 10^8$	8.8(3)		−2.0(2)	
No. of transitions	8571		11315	
RMS Dev.	0.00024		0.00029	
J_{max}	77		62	
K_{max}	71		61	

[a] $\Delta B = B' - B''$, $\Delta C = C' - C''$, etc.

[b] Values of uncertainties (two standard deviations) are given in parentheses. All band centers should be given an additional uncertainty of $0.00015\ cm^{-1}$ to account for calibration uncertainty.

[c] Fitted data for ν_{10} came from the ν_{10} fundamental and from the $\nu_{10}-\nu_{18}$ hot bands. Rotational level differences for ν_{18} came from combination–differences involving $\nu_{10} - \nu_{18}$, $\nu_{11} - \nu_{18}$, and $\nu_{18} + \nu_{15} - \nu_{18}$ hot bands. Additional vibrational-rotational levels of ν_{18} were obtained from $\nu_{10} - (\nu_{10} - \nu_{18})$, $\nu_{11} - (\nu_{11} - \nu_{18})$ and $(\nu_{18} + \nu_{15}) - (\nu_{18} + \nu_{15} - \nu_{18})$ differences.

The ν_{10} (e') − ν_{18} (e'') difference band, seen in Fig. 3, is an interesting case of a parallel band between two degenerate states. Since Δl and $\Delta k = 0$ for the transitions, the spectrum is a superposition of P–Q–R branches for the $kl < 0$ and $kl > 0$ cases and this gives rise to the two distinct Q-branch features apparent in the spectrum. Although the spectrum is heavily congested, knowledge of the experimental ν_{10} rovibrational parameters, coupled with good estimates of the ν_{18} constants from the Gaussian results, made possible a confident assignment and analysis of almost 3500 transitions. However, additional information about the ν_{18} levels is contained in the $\nu_{11} - \nu_{18}$ and $(\nu_{15} + \nu_{18}) - \nu_{18}$ difference bands, and the following iterative strategy was adopted to take advantage of this. This involved using the ν_{18} parameters from the $\nu_{10} - \nu_{18}$ fit in the initial analysis of the $\nu_{11} - \nu_{18}$ and $(\nu_{15} + \nu_{18}) - \nu_{18}$ difference bands and then, in the final iteration at the end, all transitions involving ν_{18} levels were used in a combination–difference analysis to obtain the set of ν_{18} rovibrational parameters presented in Table 4. This procedure avoided any contamination of the ν_{18} constants that could be caused by potential perturbations in the ν_{10}, ν_{11}, and $\nu_{15} + \nu_{18}$ levels. Such perturbations are particularly troublesome in the case of the ν_{11} levels, due to the strong Coriolis interactions with ν_{14} levels, as described below. The details of the $(\nu_{15} + \nu_{18}) - \nu_{18}$ band will be given with an accompanying analysis of the $(\nu_{15} + \nu_{18})$ combination band in a subsequent paper.

The experimental values for the rovibrational parameters ΔB, ΔC, $(C\zeta)$ and q of ν_{18} are in excellent agreement (1–3%) with the theoretical results. Such agreement is representative of what we have observed in other cases where the levels are unperturbed by interaction with nearby states. However the ν_0 value predicted from the anharmonic calculations ($682.6\ cm^{-1}$) is 5% lower than the actual value ($717.12\ cm^{-1}$), a difference that is significantly larger than the 0 to 2% difference seen for most other vibrational modes of propellane (see Table 2). The other exception in propellane is the ν_{15} (a_2'') mode for which the theoretical value is low by 7.5%. Neither ν_{15} nor ν_{18} is involved in a Fermi resonance and, in both cases, examination of the Gaussian output shows that the largest anharmonicity correction comes from the cubic contribution to the anharmonic coupling term with the ν_3 mode, with significant additions from coupling with ν_{11} and ν_{16}. All of these modes have significant skeletal motions involving the novel axial CC bond of propellane. It would be interesting to see if quantum calculations using different methods and basis sets could give anharmonic constants that are in better agreement with the experimental results.

4.4. ν_{11} and ν_{14} analysis

The ν_{14} mode shown in Fig. 1 appears to be nearly pure CH_2 wagging motion but the normal mode calculations of Ref. [10] indicate that about 19% mixing occurs with ν_{15}, a mode involving movement along the symmetry axis of the axial CC bond with respect to the equatorial plane. From Ref. [10], the degenerate ν_{11} motion is mainly an e'-type distortion of the C_{eq}–C_{ax} bonds (51%) with about 17% of CH_2 rocking motion, with the latter overemphasized in the GaussView representation shown in Fig 1.

According to both the Gaussian calculations and the assignments given by Wiberg et al. [10], ν_{11} is expected to be 10 or $20\ cm^{-1}$ below ν_{14} and, indeed, a weak ν_{11} Q-branch can be seen in the intense P-branch of ν_{14} about $13\ cm^{-1}$ below the ν_{14} Q-branch, Fig. 7. The Gaussian calculations also predict that the rotational levels of those two states should be coupled by a Coriolis constant with a value of approximately $w_{1,1} = 0.087\ cm^{-1}$. Even though the expected constants for the two states indicate that there will be no overlapping of levels that can be directly connected through the $w_{1,1}$ constant, such a large coupling between states that are so close would be expected to cause complications

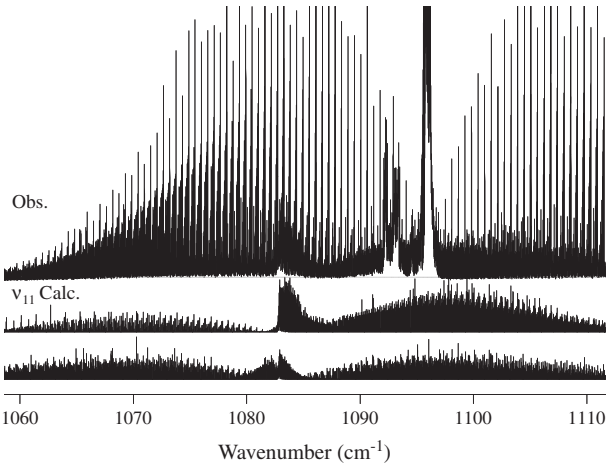

Fig. 7. The ν_{11} band that is visible within the region of the strong ν_{14} band. The top trace shows the strong ν_{14} band (1096 cm^{-1}) and weak ν_{11} band (1083 cm^{-1}). The middle (calculated) trace, shows the effect of the Coriolis interaction on the intensities of the ν_{11} band; in the bottom trace, that effect is not included.

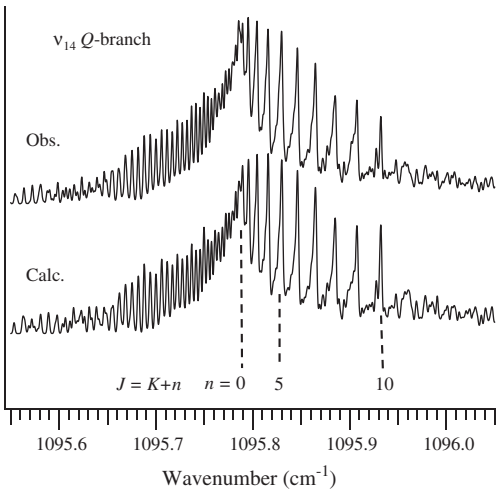

Fig. 9. The Q-branch region at the center of the ν_{14} band. The $J = K + n$ subband heads are indicated for $n = 0$–10.

that cannot be ignored. For that reason the analysis of those two states proceeded in tandem with the inclusion of the $w_{1,1}$ term in the Hamiltonian and also as a variable in the least-squares fit. As seen at the bottom of Fig. 7, this mixing is necessary to properly account for the intensity distribution seen for ν_{11}.

The assignment of the low-J and low-K transitions of the parallel band of ν_{14} was quite straightforward, especially given the nuclear spin statistics which cause lines for lower state levels with K divisible by 3 to be stronger than the others. Fig. 2 gives an overview of the ν_{14} band as well as that of ν_{10} and ν_{11}. It is obvious that the ν_{14} band is much stronger than either ν_{10} or ν_{11}. In fact the lines of ν_{11} are easily confused with lines from hot bands such as $(\nu_{12} + \nu_{14}) - \nu_{12}$ and $(\nu_{15} + \nu_{14}) - \nu_{15}$ that must accompany the transitions from the ground state to the ν_{14} state. When the ν_{14} band is spread out as, for example, in Fig. 8, the lines of ν_{14} with K = multiples of 3 are generally obvious. This intensity enhancement due to nuclear spin statistics also produces what appears to be an alternation in intensity of the P- and R-branch clusters in Fig. 2. This is caused by alternation of the intensity of the $K = 0$ transitions due to the greater statistical weight given the J'' = odd transitions from levels with A_2' or A_2'' rovibrational symmetry.

As shown in Fig. 9 the central Q-branch of ν_{14} does not have a sharp edge as is often the case for parallel bands. Instead there is a series of subband heads with each subband consisting of transitions for which $J = K + n$. The subband heads occur at increasing wavenumbers as the value of n increases. The last recognizable subband head is at 1095.933 cm^{-1} which corresponds to the

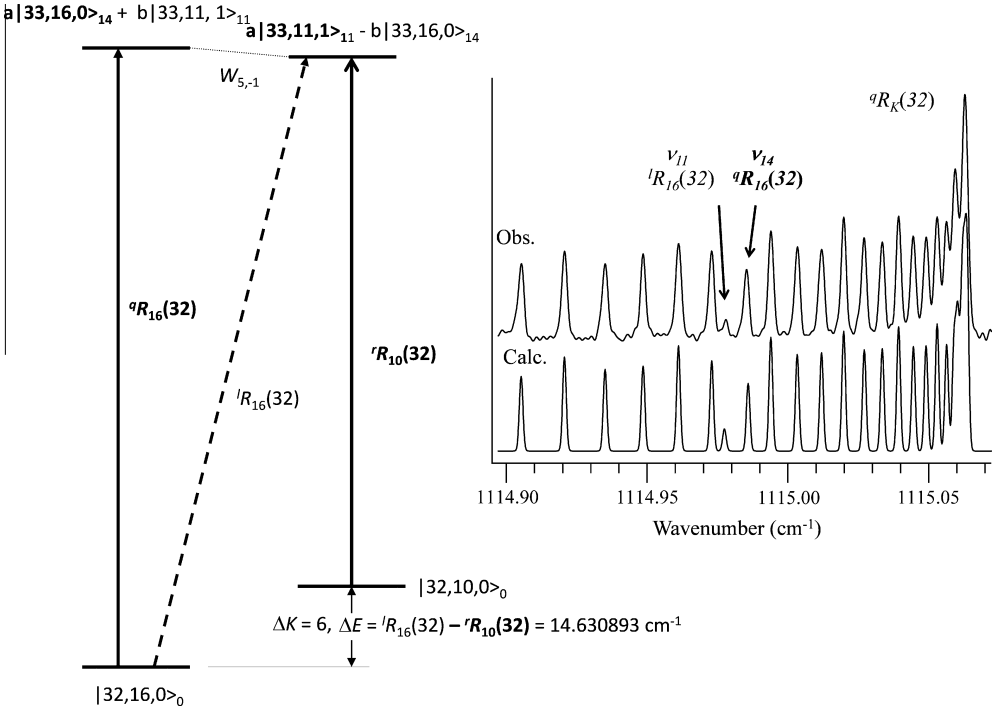

Fig. 8. The R-branch cluster of ν_{14} with level diagram showing the interaction of upper state levels. Mixing of the $J' = 33$, $K' = 16$ level of ν_{14} with the $J' = 33$, $K' = 11$ level of ν_{11} produces the weak ν_{11} feature which appears due to intensity transfer from ν_{14}.

$^qQ_{37}(47)$ transition with $n = 10$. To the red of the band center there is a nice series of lines that even show a slight strong-weak-weak-strong... alternation in intensity. While largely overlapped with other transitions, the strongest component of each line is the transition with $J = K$ and the slightly stronger transitions are the ones with K divisible by 3. Since all of the transitions in the Q-branch region are overlapped, no ν_{14} Q-branch transitions were used in the least-squares fits. Even so, the nice agreement between the calculated and observed spectrum in Fig. 9 gives confidence that the assignments are correct.

The assignment of the transitions for the ν_{11} band were more difficult, in part because of their low intensity and in part because they were easily confused with hot band transitions that accompany the ν_{14} band. Instead, the more easily assigned difference band, $\nu_{11} - \nu_{18}$, near 365 cm^{-1} was used to help determine the constants for ν_{11}. Since the constants for ν_{18} had already been determined from the fit of the $\nu_{10} - \nu_{18}$ band, the constants for ν_{11} were well determined from the analysis of the $\nu_{11} - \nu_{18}$ band. The fit of 2970 lines of that difference band had an RMS dev. of 0.000280 cm^{-1}. With the analysis of the difference band, the assignments of many ^rR transitions of ν_{11} in the region from 1098 to 1110 cm^{-1} become quite obvious and unambiguous. Most of the transitions for the ν_{11} band are ^rR-transitions but several hundred ^pP- transitions have been found and the $kl < 0$ levels of ν_{11} are well-represented among the transitions in the $\nu_{11} - \nu_{18}$ band.

While most of the transitions observed for the ν_{14} band are easily calculated without including any complications beyond the small effect of the $\Delta k = \pm1$, $\Delta l = \pm1$ interaction between the levels of the ν_{14} state and the levels of the ν_{11} state, there are a few levels of ν_{14} that are obviously perturbed, especially at high J values. The spectrum displayed in Fig. 8 shows one example of a perturbed transition, namely the $^qR_{16}(32)$ transition of ν_{14} is displaced to higher wavenumbers by about 0.0012 cm^{-1}. About 0.008 cm^{-1} below it is the weak $^lR_{16}(32)$ transition of ν_{11} that has borrowed intensity from $^qR_{16}(32)$. An identical pattern is found in the corresponding $^qP_K(34)$ cluster region. As seen in the level diagram of Fig. 8, these perturbations are caused by a near coincidence of the $J = 33$, $K = 16$ level of ν_{14} and the $J = 33$, $k = 11$, $l = 1$ level of ν_{11}. Those two levels have the same rovibrational symmetry and so they can interact, although the coupling constant is small. The shifts caused by this interaction can be reproduced by means of the $\Delta k = \pm5$, $\Delta l = \mp1$ matrix element given by Eq. (8). As confirmation of this picture, the $^rR_{10}(32)$ transition of ν_{11}, which occurs elsewhere, is displaced by the same amount as $^qR_{16}(32)$, but in the opposite direction. An important consequence of these observations is that they allow an accurate determination of the C_0 constant, as discussed below.

Further investigation shows that the $J = 45$, $K = 17$, $l = 0$ level of ν_{14} should also be very close to the $J = 45$, $K = 12$, $l = 1$ level of ν_{11}. Fig. 10 shows that perturbation in the $^qR_K(44)$ cluster of lines in the spectrum of the ν_{14} band and it can be seen that the $^qR_{17}(44)$ transition of ν_{14} is displaced to higher wavenumbers by about 0.0042 cm^{-1}, causing the apparent enhanced intensity of the overlapping $K = 16$ transition Note that, since J is higher in value, the off-diagonal coupling term should be larger, hence the greater shift than observed for the $J = 33$ case above.

In the P-branch region of ν_{14} there is an "extra" line at 1069.766 cm^{-1} which is believed to be the $^lP_{17}(46)$ line of ν_{11} which has borrowed intensity from the $^qP_{17}(46)$ line of ν_{14}. In a manner analogous to that shown in Fig. 8, this transition can be combined with the $^rR_{11}(44)$ transition of ν_{11} to give a ground state difference of 36.519822 cm^{-1} between the levels $J = 46$, $K = 17$ and $J = 44$, $K = 11$. Other, similar, combinations involving different K values have been formed for the ground state; these are given in Table 7.

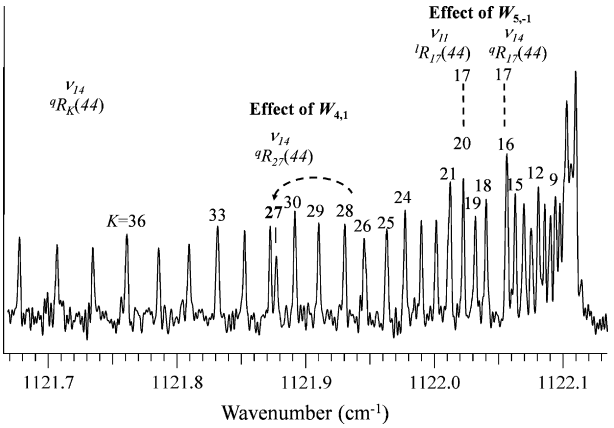

Fig. 10. The R-branch cluster for $J'' = 44$ of ν_{14}. Two areas of perturbations can be seen. The $K'' = 27$ transition is shifted due to a $\Delta k = \pm4$, $\Delta l = \pm1$ interaction with ν_{16}. The $K'' = 17$ transition is split due to a $\Delta k = \pm5$, $\Delta l = \mp1$ interaction with ν_{11} and overlaps with the $K'' = 16$ and 20 transitions.

The same $W_{5,-1}$ perturbation has been found to affect the $^qR_{17}(44)$ transition of ν_{14} and the $^rR_{11}(44)$ transition of ν_{11}. The adjacent higher-J and lower-J transitions are also very slightly affected. Two other avoided crossings are predicted to occur, one at $J = 15$, $K = 15$ of ν_{14} and another at $J = 55$, $K = 18$. The first would be at such a low value of J that it would be too weak to be detected. The second involves a ν_{11} region where there are several other perturbations and so the assignments are rather confusing and uncertain. The effects are seen in the ν_{14} spectra however and our model does account for the observations. (More details can be found in Ref. [14], Fig. 4.18.)

Also seen in Fig. 10 is a large displacement to the red of the $J = 45$, $K = 27$ level. That perturbation is believed to involve the $J = 45$, $kl = 31$ level of ν_{16} and requires a $\Delta k = \pm4$, $\Delta l = \pm1$ matrix element as given by Eq. (7). Other observed displacements of the P- and R-branch lines shows that there are six avoided-crossing points beginning at

a. $J = 38$, $K = 30$ of ν_{14} and $J = 38$, $kl = 34$ of ν_{16}.
b. $J = 40$, $K = 29$ of ν_{14} and $J = 40$, $kl = 33$ of ν_{16}.
c. $J = 43$, $K = 28$ of ν_{14} and $J = 43$, $kl = 32$ of ν_{16}.
d. $J = 45$, $K = 27$ of ν_{14} and $J = 45$, $kl = 31$ of ν_{16}.
e. $J = 47$, $K = 26$ of ν_{14} and $J = 47$, $kl = 30$ of ν_{16}.
f. $J = 49$, $K = 25$ of ν_{14} and $J = 49$, $kl = 29$ of ν_{16}.

Although the transitions at the crossing points are the most affected, the transitions involving adjacent levels are also affected so there are many more than just six perturbed transitions. Because we have explicitly included $W_{4,1}$ and $W_{5,-1}$ terms in our fitting model, all these perturbations are treated in the analysis.

Tables 5 and 6 give the constants obtained from the least-squares fit of both the ν_{11} and ν_{14} bands as well as the $\nu_{11} - \nu_{18}$ difference band, including parameters describing the ν_{11}/ν_{14} interactions as well as parameters for interaction of ν_{14} with the ν_{16} state. Note that transitions from the ground state to ν_{16} are IR-inactive so the values given for ν_{16} are derived from the effect the ν_{14}/ν_{16} interaction has on ν_{14}. It is also expected that ν_3 is nearby and will certainly have a strong effect on the rotational levels of ν_{16}. Consequently the constants given for ν_{16} in Table 6 are only effective constants required to account for the observed perturbations to levels of ν_{14}, and these constants may be quite different from those that would be given by a complete treatment of the interaction of ν_{16} with the other nearby levels. This may account for the poorer agreement between theory and experiment seen for the ΔB and ΔC parameters of ν_{11}, ν_{14}, and ν_{16}, compared to

Table 5
Rovibrational parameters (cm^{-1}) of the ν_{11} and ν_{14} vibrational states of propellane.[a]

Constant[b]	ν_{11}		ν_{14}	
	Expt.	Theory	Expt.	Theory
ω_0		1101.2		1120.0
ν_0	1082.90413(3)	1071.4	1095.78687(4)	1091.8
$\Delta C \times 10^3$	−0.04074(18)	−0.258	−0.1018(2)	−0.110
$\Delta B^* \times 10^3$	−0.3451(30)	0.593	−0.295(6)	−0.996
$\Delta D_J \times 10^7$	0.103(7)		−0.185(12)	
$\Delta D_{JK} \times 10^7$	0.430(13)		−1.629(21)	
$\Delta D_K \times 10^7$	−1.636(16)		1.815(29)	
$\Delta H_J \times 10^{11}$	0.018(6)		−0.066(6)	
$\Delta H_{JK} \times 10^{11}$	0.660(19)		−0.601(16)	
$\Delta H_{KJ} \times 10^{11}$	−5.413(29)			
$\Delta H_K \times 10^{11}$	10.871(25)		0.669(21)	
$\Delta_2 \times 10^8$	−1.716(11)			
$\Delta_3 \times 10^{12}$			−0.428(4)	
$C\zeta^{(z)}$	−0.0595596(21)	−0.0694		
$\eta_J \times 10^5$	−0.078(11)			
$\eta_K \times 10^5$	−0.563(11)			
$\eta_{JK} \times 10^9$	0.496(26)			
$\eta_{KK} \times 10^9$	−2.992(27)			
$\eta_{JKK} \times 10^{12}$	1.223(8)			
$\eta_{KKK} \times 10^{12}$	−1.981(8)			
$q^* \times 10^3$	0.530(6)	0.162		
$q_J \times 10^8$	0.54(11)			
$q_K \times 10^8$	7.76(5)			
No. of transitions	4325		3413	
RMS Dev.	0.00027		0.00022	
J_{max}	54		71	
K_{max}	49		62	

[a] Parameters given are from a fit that included ν_{16} and the interaction parameters in Table 6.
[b] The * on D*B* and *q* indicates that these have been "deperturbed" by explicitly including the off-diagonal $W_{1,1}$ interaction between ν_{11} and ν_{14}.

Table 6
Some interaction and rovibrational parameters (cm^{-1}) of propellane.

Constant[a]	Expt.	Theory
ν_{11}, ν_{14} interaction parameters		
$w_{1,1}$	0.0640(3)	0.087
$w_{1,1J} \times 10^4$	−0.0193(5)	
$w_{1,1K} \times 10^4$	−0.0380(8)	
$w_{1,1,kl} \times 10^4$	2.00(11)	
$w_{5,-1} \times 10^9$	−3.74(13)	
$w_{5,-1J} \times 10^{12}$	−0.72(4)	
$\eta_{5,-1K} \times 10^{12}$	1.7(3)	
ν_{16}, ν_{14} interaction parameters		
$w_{4,1} \times 10^8$	5.701(11)	
$w_{4,1J} \times 10^{11}$	−0.709(2)	
ν_{16} rovibrational parameters		
ω_0		1151.7
ν_0	1122.481(9)	1119.5
$\Delta C \times 10^3$	0.074(8)	−0.1040
$\Delta B \times 10^3$	−2.784(3)	0.3790
(Cz)	0.0622(6)	0.0624
$\eta_J \times 10^5$	1.46(4)	
$\eta_K \times 10^5$	4.32(6)	

[a] These parameters were included in the fit that gave the results in Table 5.

the results for ν_{10} and ν_{18}. Better agreement is seen for $(C\zeta)_{16}$ and $(C\zeta)_{11}$ parameters, probably because these values are mainly determined by the ζ values, which depend only on quadratic force constants. The calculated anharmonic vibrational frequencies are within 1% of the observed values and it may be significant that these modes do not involve as much disturbance of the unusual axial bond of propellane as do the ν_{15} and ν_{18} modes mentioned earlier.

4.5. A_1, A_2 splittings

Four different types of splittings were observed in the present work: (1) the usual *l*-type doubling splitting represented by the parameter q_v, (2) the splitting of the $K = 3$ levels of the non-degenerate vibrational states represented by the parameter Δ_3, (3) the splitting of the $kl = -2$ levels of the degenerate vibrational states represented by the constant Δ_2, and (4) the splitting of the $kl = 4$ levels in the three degenerate vibrational states, ν_{10}, ν_{11}, and ν_{18}. The first three splittings are directly calculated by using different splitting terms as presented in Eqs. (2) and (5). The small $kl = 4$ splitting for the degenerate states does not require, for example, a Δ_4 splitting term, since it can be reproduced by propagation of the larger splitting of the $kl = -2$ levels to the $kl = 4$ levels via the $\Delta k = \pm 2$, $\Delta l = \pm 2$ matrix element, Eq. (5).

These splitting constants can only be given signs when the intensities are considered. In this paper we have used the convention that the splitting constant is positive if the A_1' or A_1'' rovibrational levels are above (below) the A_2' or A_1'' levels for even (odd) values of *J*. The different nuclear spin statistics allow us to determine which are the A_2 levels because transitions involving them are stronger by a factor of two, as shown in Fig. 6.

We note that the Gaussian value for $\Delta_3 = h_3$ of the ground state is quite small, 0.118×10^{-13} cm^{-1}, and an accurate value for this could not be determined from the experimental fits. Accordingly, it was set to zero in obtaining the parameters listed in the tables. It is interesting that the same constant for the splitting of the $K = 3$ levels of the ν_{14} state is nearly forty times greater than the Gaussian value for the ground state. One might expect that the $w_{1,1}$ constant which couples the $kl = -2$ levels of E' states to the $K = 3$ levels of A_2'' states would result in a measureable splitting of those $K = 3$ levels as is observed for ν_{14}. However, since we have already included explicitly this coupling between ν_{14} and ν_{11}, the residual splitting represented by Δ_3 must come from the coupling between ν_{14} and the other E' states such as ν_{10}, which has been ignored in this analysis.

Just as the value of *q* reflects the accumulated effects of the $w_{1,1}$ parameters coupling the $kl = 1$ levels of E' states with the $K = 0$ levels of A'' states, so the value of Δ_2 could be considered to reflect the $w_{2,-1}$ coupling of the $kl = -2$ levels of E' states and the $K = 0$ levels of A' states. The Δ_2 values for ν_{10} and for ν_{18} are both negative and on the order of 10^{-8} cm^{-1}. The unusually large value of Δ_2 for ν_{11} may be due in part to the closeness of ν_3 even though there is no other sign of any coupling between ν_{11} and ν_3.

The $kl = 4$ levels for the three degenerate states studied here are split as a result of the coupling to the split $kl = -2$ levels through the q_v term given in Eq. (5). That coupling will result in the same A_1, A_2 ordering as found for the $kl = -2$ levels. Since the three Δ_2 constants are all negative, then for even *J* levels of ν_{10}, ν_{11}, and ν_{18} the, A_2 levels will be above the A_1 levels in both the $kl = -2$ and the kl = 4 levels.

Finally, for the degenerate vibrational modes we have studied here and in Refs. [12,13], the signs we assign to q_v according to our convention and to the observed intensities are (in parentheses) $q_9(+)$, $q_{10}(-)$, $q_{11}(+)$, $q_{12}(-)$ and $q_{18}(-)$. The magnitudes of values (Tables 4 and 5 and Refs. [12,13]) fall in the range 10^{-4} to 10^{-3} cm^{-1}. The values we deduce from the Gaussian results using the method described in Ref. [25] are generally consistent with the experimental magnitudes, particularly in cases such as ν_{18} and ν_{10} where coupling with other states is minimal. The signs deduced from the Gaussian output also agree with our experimental signs for q_{10}, q_{11}, and q_{18} but are opposite for q_9 and q_{12}, for reasons unknown to us.

4.6. Determination of C_0

It is well known that the normally-allowed fundamental infrared transitions for a symmetric top molecule cannot be used to

Table 7
Ground state combination–differences that help to determine C_0 and D_K.

Energy difference (cm^{-1})	Obs. − calc. (cm^{-1})	J'	K'	J''	K''	Transitions used[a]
14.62814	−0.00025	34	10	34	16	$^{q}R_{16}(34) - {}^{w}R_{10}(34)\ \nu_{14}$
14.63049	−0.00052	32	10	32	16	$^{q}R_{16}(32) - {}^{w}R_{10}(32)\ \nu_{14}$
14.63089	−0.00012	32	10	32	16	$^{l}R_{16}(32) - {}^{r}R_{10}(32)\ \nu_{11}$
15.73687	−0.00047	44	11	44	17	$^{l}R_{17}(44) - {}^{r}R_{11}(44)\ \nu_{11}$
15.73753	0.00019	44	11	44	17	$^{q}R_{17}(44) - {}^{w}R_{11}(44)\ \nu_{14}$
23.87248	0.00037	34	16	32	10	$^{r}R_{10}(32) - {}^{l}P_{16}(34)\ \nu_{11}$
23.87259	0.00048	34	16	32	10	$^{w}R_{10}(32) - {}^{q}P_{16}(34)\ \nu_{14}$
36.51923	−0.00053	46	17	44	11	$^{w}R_{11}(44) - {}^{q}P_{17}(46)\ \nu_{14}$
36.51982	0.00006	46	17	44	11	$^{r}R_{11}(44) - {}^{l}P_{17}(46)\ \nu_{11}$
53.13122	−0.00029	34	10	32	16	$^{q}R_{16}(32) - {}^{w}R_{10}(34)\ \nu_{14}$

[a] The left superscripts *w* and *l* on the transitions correspond to $\Delta K = +6$ and -5, respectively.

determine any purely *K*-dependent constants. However, under certain circumstances [20], especially when Coriolis interactions mix different *K* levels, the values of C_v and sometimes D_K and H_K can be determined. In the present case, ν_{14} is coupled to both ν_{16} and ν_{11} by rovibrational interactions that mix levels with different values of *k*. In the case of ν_{16} there are no IR-active transitions from the ground state so the coupling does not give rise to any new transitions for ν_{14} or in any other way allow one to determine any purely *K*-dependent constants. However the coupling of levels of ν_{11} and ν_{14} do provide such an opportunity.

As indicated above there are some avoided-crossings of levels of ν_{14} and ν_{11} that have the same rovibrational symmetry and so the associated states can interact. If the levels are close enough together they will be significantly shifted and mixed. As explained earlier, Figs. 8 and 10 show two examples of transitions displaced by such crossings and the level diagram of Fig. 8 is illustrative . To reproduce both cases the $\Delta k = \pm 5$, $\Delta l = \mp 1$ off-diagonal matrix element (Eq. (8)) is required in the Hamiltonian and the separation of the two interacting levels must be known. The correct values for C_0 and D_K are required in order to know the separation of the coupled levels and hence should be determinable.

Because most of the constants for both ν_{11} and ν_{14} have been determined from allowed transitions from the ground state, the analysis of the perturbed transitions requires a determination of the higher-order Coriolis interaction constant, $w_{5,-1}$, and C_0, D_K and possibly H_K. One way to determine the ground state constants without inclusion of $w_{5,-1}$ is to make use of ground state combination–differences based in part on normally forbidden, but perturbation allowed, transitions. As indicated in Table 7 ten ground state combination–differences have been found that connect levels with different values of *K*. Fitting these combination–differences yields a value of 0.1936526(8) cm^{-1} for C_0 but the limited range of *K* does not permit a determination of D_K or H_K. However with the explicit inclusion of the $w_{5,-1}$ parameter, the much larger full set of data for ν_{11} and ν_{14} samples a broader *K*-range and fitting of the small but measurable shifts is possible. There results a nearly identical value of $C_0 = 0.1936515(4)$ and a value of $D_K = 0.4199(13)$ cm^{-1}, both in excellent agreement (within 1%) with values from the theoretical calculations. Attempts were made to fit also the ground state H_K parameter but the uncertainty was large, hence this parameter was fixed at the Gaussian value in obtaining the above results.

The complete determination of the four structural parameters of propellane (bond lengths C_{ax}–C_{eq}, C_{ax}–C_{ax}, C–H and the HCH angle) is not possible from the two rotational constants we have determined. However it is noteworthy that B_0 and C_0 are sufficient to give an accurate value for the most interesting geometric parameter, the axial CC bond length. In particular, it is easily shown that this distance $R = [(2I_b - I_c)/M]^{1/2}$ where I_b and I_c are the moments of inertia and *M* is the carbon mass. If used to relate ground state constants to a ground state structure, one obtains a value of $R = 1.586277(3)$ Å. Of course, this relation applies strictly only for the equilibrium case, and there are other problems involved in deducing structures from spectroscopic measurements [27]. Nonetheless, the value obtained is in very good agreement with a thermal average value of 1.596(5) Å obtained in an electron diffraction study [9] and the bond length is noticeably longer than the more normal C_{ax}–C_{eq} bond length of 1.525(2) Å determined in that study.

5. Summary

The analysis has given accurate rovibrational constants for ν_{10} and ν_{18} modes of propellane and a model is presented in which various Coriolis interactions are included to extract similar parameters for the ν_{11} and ν_{14} modes. Localized perturbations in ν_{11}, ν_{14} spectra permit the determination of the C_0 rotational constant and lead to a determination of the bond length of the unusual axial CC bond in propellane. Comparisons of the experimental and theoretical rovibrational parameters are generally favorable although the agreement degrades as the number of interacting states increases. This feature becomes increasingly apparent as one goes to higher vibrational frequencies where the density of combination-state levels becomes greater. This aspect, and the determination of some of the anharmonicity constants of propellane, will be the subject of a forthcoming paper.

Acknowledgments

R. Kirkpatrick is grateful to Oregon State University for Milton Harris, Benedict, and Shoemaker Fellowships during the course of this PhD thesis work [14]. J. Nibler acknowledges the support of the Camille and Henry Dreyfus Foundation in the form of a Senior Scientist Mentor Award. The research described here was performed, in part, in EMSL, a national scientific user facility sponsored by the Department of Energy's Office of Biological and Environmental Research and located at Pacific Northwest National Laboratory (PNNL). PNNL is operated for the United States Department of Energy by the Battelle Memorial Institute under contract DE-AC05-76RLO 1830. We thank Robert Sams for helpful advice and assistance in recording the infrared spectra of propellane in this facility, and Tim Hubler, also at PNNL, for his expert advice on synthesis techniques.

Appendix A. Supplementary material

Supplementary data for this article are available on ScienceDirect www.sciencedirect.com) and as part of the Ohio State University Molecular Spectroscopy Archives (http://msa.lib.ohiostate.edu/jmsa_hp.htm). Supplementary data associated with this article can be found, in the online version, at http://dx.doi.org/10.1016/j.jms.2012.09.001.

References

[1] R. Kirkpatrick, T. Masiello, N. Jariyasopit, A. Weber, J.W. Nibler, A. Maki, T.A. Blake, T. Hubler, J. Mol. Spectrosc. 248 (2008) 153–160.

[2] J. Altman, E. Babad, J. Itzchaki, D. Ginsburg, Tetrahedron 22 (Suppl. 8) (1966) 279–304;
D. Ginsburg, Accounts Chem. Res. 2 (1969) 121.

[3] D. Ginsburg, Propellanes-Structure and Reactions, Verlag Chemie, Weinheim, 1975 (and references to earlier works contained therein);
D. Ginsburg, in: B. Christoph (Ed.), Topics of Current Chemistry-Organic Synthesis, Reactions, and Mechanisms, vol. 137, 1987, pp. 1–17.;
K.B. Wiberg, Chem. Rev. 89 (1989) 975–983.

[4] F. Vögtle, Fascinating Molecules in Organic Chemistry, John Wiley, Chichester, 1992.

[5] H. Hopf, Classics in Hydrocarbon Chemistry: Synthesis, Concepts, Perspectives, Wiley-VCH, Weinheim, 2000.

[6] H. Dodziuk, Modern Conformational Analysis: Elucidating Novel Exciting Molecular Structures, VCH Publishers, Inc., New York, 1995.

[7] E.L. Eliel, S.H. Wilen, Lewis N. Mander, Stereochemistry of Organic Compounds, Wiley and Sons, Inc., New York, 1994.

[8] M.D. Levin, P. Kaszynski, J. Michl, Chem. Rev. 100 (2000) 169–234.

[9] L. Hedberg, K. Hedberg, J. Am. Chem. Soc. 107 (1985) 7257–7260.

[10] K.B. Wiberg, W.P. Daley, F.H. Walker, S.T. Waddell, L.S. Crocker, M. Newton, J. Am. Chem. Soc. 107 (1985) 7247–7257.

[11] K.B. Wiberg, F.H. Walker, J. Am. Chem. Soc. 104 (1982) 5239–5240.

[12] R. Kirkpatrick, T. Masiello, N. Jariyasopit, J.W. Nibler, A. Maki, T.A. Blake, A. Weber, J. Mol. Spectrosc. 253 (2009) 41–50.

[13] A. Maki, A. Weber, J.W. Nibler, T. Masiello, T.A. Blake, R. Kirkpatrick, J. Mol. Spectrosc. 264 (2010) 26–36.

[14] R. Kirkpatrick, Examination of Low-Lying Rovibrational States of D3h Oblate Top Molecules using High-Resolution FTIR and Coherent Anti-Stokes Raman Spectroscopies, PhD thesis, Oregon State University, December 2010.

[15] G. Herzberg, Molecular Spectra and Molecular Struture, vol. 2, Infrared and Raman Spectra of Polyatomic Molecules, van Nostrand Reinhold Co., New York, NY, 1962 (p. 434).

[16] J. Belzner, U. Bunz, K. Semmler, G. Szeimies, K. Opitz, A.-D. Schluter, Chem. Ber. 122 (1989) 397–398;
See also K. Semmler, G. Szeimies, J. Belzner, J. Am. Chem. Soc. 107 (1985) 6410–6411.

[17] F. Alber, G. Szeimies, Chem. Ber. 125 (1985) 757–758.

[18] C. Di Lauro, I.M. Mills, J. Mol. Spectrosc. 21 (1966) 363–413.

[19] D. Papousek, M.R. Aliev, Molecular Vibration-Rotational Spectroscopy, Elsevier, Amsterdam, New York, 1982.

[20] A.G. Maki, T. Masiello, T.A. Blake, J.W. Nibler, A. Weber, J. Mol. Spectrosc. 255 (2009) 56–62.

[21] See Ref. 15, p. 422, 426.

[22] A. Weber, J. Chem. Phys. 73 (1980) 3952–3972.

[23] M.J. Frisch, G.W. Trucks, H.B. Schlegel, G.E. Scuseria, M.A. Robb, J.R. Cheeseman, G. Scalmani, V. Barone, B. Mennucci, G.A. Petersson, H. Nakatsuji, M. Caricato, X. Li, H.P. Hratchian, A. F. Izmaylov, J. Bloino, G. Zheng, J.L. Sonnenberg, M. Hada, M. Ehara, K. Toyota, R. Fukuda, J. Hasegawa, M. Ishida, T. Nakajima, Y. Honda, O. Kitao, H. Nakai, T. Vreven, J.A. Montgomery, Jr., J.E. Peralta, F. Ogliaro, M. Bearpark, J.J. Heyd, E. Brothers, K. N. Kudin, V. N. Staroverov, T. Keith, R. Kobayashi, J. Normand, K. Raghavachari, A. Rendell, J.C. Burant, S.S. Iyengar, J. Tomasi, M. Cossi, N. Rega, J.M. Millam, M. Klene, J.E. Knox, J.B. Cross, V. Bakken, C. Adamo, J. Jaramillo, R. Gomperts, R.E. Stratmann, O. Yazyev, A.J. Austin, R. Cammi, C. Pomelli, J.W. Ochterski, R.L. Martin, K. Morokuma, V.G. Zakrzewski, G.A. Voth, P. Salvador, J.J. Dannenberg, S. Dapprich, A.D. Daniels, O. Farkas, J.B. Foresman, J.V. Ortiz, J. Cioslowski, D.J. Fox, Gaussian 09, Revision B.01, Gaussian, Inc., Wallingford CT, 2010.

[24] A. Willets, N.C. Handy, Chem. Phys. Lett. 235 (1995) 286–290.

[25] A. Perry, M.A. Martin, J.W. Nibler, A. Maki, A. Weber, T.A. Blake, J. Mol. Spectroc. 276–277 (2012) 22–32.

[26] We thank Professor Norman Craig of Oberlin College for suggesting this method of properly orienting the axes in the Gaussian calculations.

[27] See, for example, the following chapters in the book by A. Domenicano, I. Hargittai (Eds.), Accurate Molecular Structures, their Determination and Importance, Oxford University Press, New York, 1992;
K. Kuchitsu, The Potential Energy Surface and the Meaning of Internuclear Distances, pp. 14–46 (chapter 2).;
B.P. van Eijck, Structure Determinations by Microwave Spectroscopy, chapter 3, pp. 47–64.;
G. Graner, Determination of Accurate Molecular Structure by Vibration-Rotation Spectroscopy, pp. 65–94 (chapter 4).;
I. Hargittai, Gas-Phase Electron Diffraction, pp. 95–125 (chapter 6).